Journal of Applied Physics

Systematic study of nonmagnetic resistance changes due to electrical pulsing in single metal layers and metal/antiferromagnet bilayers

Cite as: J. Appl. Phys. **128**, 173902 (2020); https://doi.org/10.1063/5.0026147
Submitted: 21 August 2020 . Accepted: 18 October 2020 . Published Online: 03 November 2020

B. J. Jacot, G. Krishnaswamy, G. Sala, C. O. Avci, S. Vélez, P. Gambardella, and C.-H. Lambert

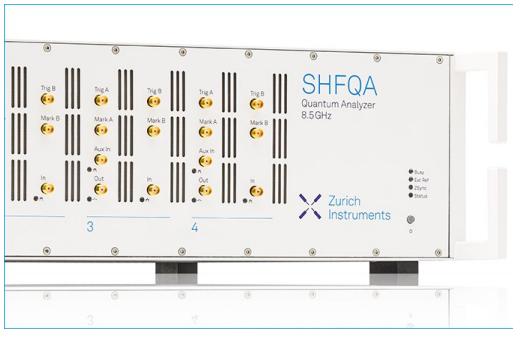

Journal of Applied Physics ARTICLE scitation.org/journal/jap

Systematic study of nonmagnetic resistance changes due to electrical pulsing in single metal layers and metal/antiferromagnet bilayers

Cite as: J. Appl. Phys. **128**, 173902 (2020); doi: 10.1063/5.0026147
Submitted: 21 August 2020 · Accepted: 18 October 2020 ·
Published Online: 3 November 2020

B. J. Jacot,[a] G. Krishnaswamy, G. Sala, C. O. Avci, S. Vélez, P. Gambardella, and C.-H. Lambert[b]

AFFILIATIONS

Department of Materials, ETH Zurich, 8093 Zurich, Switzerland

[a]**Author to whom correspondence should be addressed:** benjamin.jacot@mat.ethz.ch
[b]**Electronic mail:** charles-henri.lambert@mat.ethz.ch

ABSTRACT

Intense current pulses are often required to operate microelectronic and spintronic devices. Notably, strong current pulses have been shown to induce magnetoresistance changes attributed to domain reorientation in antiferromagnet/heavy metal bilayers and non-centrosymmetric antiferromagnets. In such cases, nonmagnetic resistivity changes may dominate over signatures of antiferromagnetic switching. We report systematic measurements of the current-induced changes of the transverse and longitudinal resistance of Pt and Pt/NiO layers deposited on insulating substrates, namely, Si/SiO_2, Si/Si_3N_4, and Al_2O_3. We identify the range of pulse amplitude and length that can be used without affecting the resistance and show that it increases with the device size and thermal diffusivity of the substrate. No significant difference is observed in the resistive response of Pt and NiO/Pt devices, thus precluding evidence on the switching of antiferromagnetic domains in NiO. The variation of the transverse resistance is associated to a thermally activated process in Pt that decays following a double exponential law with characteristic timescales of a few minutes to hours. We use a Wheatstone bridge model to discriminate between positive and negative resistance changes, highlighting competing annealing and electromigration effects. Depending on the training of the devices, the transverse resistance can either increase or decrease between current pulses. Furthermore, we elucidate the origin of the nonmonotonic resistance baseline, which we attribute to training effects combined with the asymmetric distribution of the current. These results provide insight into the origin of current-induced resistance changes in metal layers and a guide to minimize nonmagnetic artifacts in switching experiments of antiferromagnets.

I. INTRODUCTION

The compensated magnetic lattice and the strong exchange coupling between antiparallel magnetic moments make antiferromagnets (AFMs) appealing for data storage applications.[1,2] The absence of a net magnetization limits the crosstalk between devices in densely packed layouts and minimizes the influence of external magnetic fields on the magnetic order parameter. Moreover, the dynamic resonant modes associated with the staggered antiferromagnetic structure are orders of magnitude higher in frequency compared to ferromagnets,[3,4] thus opening unique prospects for terahertz spintronics.[5,6] For a long time, however, controlling the orientation of the magnetic moments in AFMs by means of scalable and integration-friendly methods was deemed to be impossible. Recent experiments provide a solution to this problem, as it was shown that the current injection in non-centrosymmetric metallic AFMs[6–16] and in heavy metal layers deposited on insulating AFMs[17–22] leads to the in-plane rotation of the Néel vector due to the current-induced spin–orbit torques.[23] Reading of the Néel vector reorientation in metallic AFMs and AFM/heavy metal bilayers can then be performed by measuring the anisotropic magnetoresistance of the AFM and spin Hall magnetoresistance of the heavy metal, respectively. Together, these effects allow for all-electrical manipulation and detection of antiferromagnetic order.

The electrical switching of AFMs requires a sufficient torque to reorient the magnetic moments, which, in turn, requires a high current density. In addition to the torque, Joule heating plays a

critical role in switching by assisting the magnetic moments in overcoming the magnetic anisotropy energy barrier between two different easy axis orientations.[10,24] Intense currents, however, can also produce irreversible changes in the materials due to thermal annealing[25] and electromigration.[26] Although the switching of the Néel vector in AFM/heavy metal bilayers such as NiO/Pt has been confirmed by imaging techniques, including x-ray photoemission electron microscopy,[17,19] birefringence,[27] and spin Seebeck microscopy,[20] transport measurements on single-layer Nb and Pt thin films have shown nonmagnetic resistive signatures very similar to the ones attributed to magnetoresistance changes.[28–30] Analogous resistive signatures in AFM/Pt bilayers are considered as a proof of current-induced switching in an increasing variety of AFMs, such as hematite,[21,22] Mn_2Au,[31] PtMn,[32] MnN,[14] Mn_3Sn,[16] and synthetic antiferromagnets.[33] Given the multiple factors that influence the resistivity of these bilayers, it is important to investigate the pulsing conditions and device characteristics that lead to the appearance of nonmagnetic resistance changes in metallic systems containing AFMs or not.

In this study, we perform a systematic characterization of the current-induced resistance changes in Pt and NiO/Pt cross-shaped devices deposited on different substrates. We report measurements of the transverse and longitudinal resistance as a function of the amplitude and length of the current pulses, device size, and training history. In agreement with the nonmagnetic resistive effects revealed by previous studies,[28–30] we show that both gradual and step-like resistance changes can be induced in Pt depending on the training of the devices and independently of the presence of NiO. Therefore, the resistance variations in NiO/Pt cannot be considered as signatures of domain switching in NiO. Using a simple Wheatstone bridge model, we identify competing effects that either decrease or increase the local resistivity, which we attribute to current-induced annealing and electromigration, respectively. Moreover, we show that the resistance changes depend strongly on the pulse length and training history of the devices as well as on the device size, which results in a broad variety of resistive signals.

This paper is organized as follows: Section II describes the pulsing and readout schemes commonly employed in AFM devices and in this work. Sections III and IV introduce the Wheatstone bridge model used to interpret the nonmagnetic resistance changes and the experimental systems, respectively. Sections V and VI present the behavior of the transverse resistance upon an application of pulses of increasing amplitude and the relaxation process after excitation. Sections VII and VIII report the device response as a function of the pulse length and substrate thermal diffusivity. Sections IX and X focus on the influence of the device size in the presence of artifacts and how asymmetric responses between two pulsing directions affect the behavior of the transverse resistance.

II. ELECTRICAL WRITING AND READING SCHEME OF ANTIFERROMAGNETS

In metallic AFMs with a non-centrosymmetric crystal structure, switching is usually ascribed to the inverse spin galvanic effect.[34] Owing to spin–orbit coupling and the lack of inversion symmetry, the electric current flowing in these AFMs generates a non-equilibrium spin polarization of opposite sign on each magnetic sublattice. The resulting staggered torque tends to align the Néel vector perpendicular to the current. Reversible switching can be achieved by pulsing along two orthogonal directions, thus inducing a rotation of $\pm 90°$ of the Néel vector. This manipulation of the magnetic orientation can then be electrically detected via a transverse magnetoresistance measurement.[7] The inverse spin galvanic effect was initially predicted for Mn_2Au[34] and experimentally confirmed in CuMnAs,[6–8,15] Mn_2Au,[9–12] and magnetically intercalated transition metal dichalcogenides.[13]

In insulating AFMs, the switching process relies on the spin-current transferred from an adjacent metallic layer with strong spin–orbit coupling. The latter scheme is similar to spin–orbit torque switching demonstrated for a metallic ferromagnet[35] and insulating ferrimagnets.[23,36] Several mechanisms have been proposed in order to explain the perpendicular switching of AFMs due to a non-staggered spin torque. In NiO(001)/Pt bilayers, it was suggested that the damping-like spin–orbit torque originating from the current-induced spin accumulation at the Pt interface induces coherent switching of antiferromagnetic domains by orienting the Néel vector toward the writing current.[18] Alternatively, the field-like spin–orbit torque acting on the uncompensated interfacial spins of NiO could drive a coherent rotation of the spins perpendicular to the writing current in Pt/NiO(111)/Pt trilayers.[17] Finally, mechanisms based on the action of the spin current on antiferromagnetic domain walls have been suggested in NiO/Pt.[19,20,37] A spin current would directly act on the magnetic moments in the domain walls, driving walls with opposite chirality in opposite directions.[38] As this process does not discriminate between the expansion or contraction of domains, an additional degeneracy-breaking mechanism is required in order to achieve net switching. The latter is provided by a translational ponderomotive force due to the damping-like torque, which favors the expansion of domains with the Néel vector parallel to the current.[19] Recently, an additional current-induced mechanism that does not involve SOT switching was proposed for a hematite/Pt bilayer deposited on Al_2O_3[21] and for NiO/Pt deposited on MgO,[39] wherein the current-induced Joule heating produces thermal expansion of the substrate and results in mechanical stress that couples to the magnetic order of the AFM through its high magnetostrictive coefficient.

All these switching mechanisms are based on a deterministic writing scheme that aligns the Néel vector either parallel or perpendicular to the writing current depending on the driving torque being damping-like or field-like, respectively, or magnetostriction. Following one or more writing pulses, an electrical readout is performed by measuring the variation of the transverse resistance. In metallic AFMs, the readout signal is the transverse component of the anisotropic magnetoresistance—also called the planar Hall effect—which is sensitive to the in-plane orientation of the Néel vector relative to the current.[7,40] In insulating AFMs adjacent to a heavy metal, the signal relates to the transverse component of the spin-Hall magnetoresistance, which is also sensitive to the in-plane orientation of the spins relative to the current direction.[41–44] The anisotropic magnetoresistance and spin-Hall magnetoresistance have the common property of being quadratic in magnetization, which means that they are invariant upon 180° reversal of the Néel vector. Both effects are extremal when the Néel vector sets at +45° (−45°) or, equivalently, at −135° (+135°) to the sensing current.

To summarize, the writing process described above accounts for 90° switching of the domains either toward or perpendicular to the writing current, and the readout signal amplitude is maximal when the sensing current flows at an angle of $\pm 45°$ from the writing line. Hence, the common device geometry is a Hall cross with either four or eight symmetrical arms. In the four arms geometry, the set writing pulse, henceforth called P1, is applied along one diagonal of the cross, whereas the reset writing pulse, henceforth called P2, is applied along the other diagonal and orthogonal to P1. During readout, a small sense current is injected between the two opposite arms of the cross, and the transverse resistance is measured by probing the Hall voltage between the two arms perpendicular to the sensing current, as illustrated in Fig. 1(a). In this work, we consider only the four

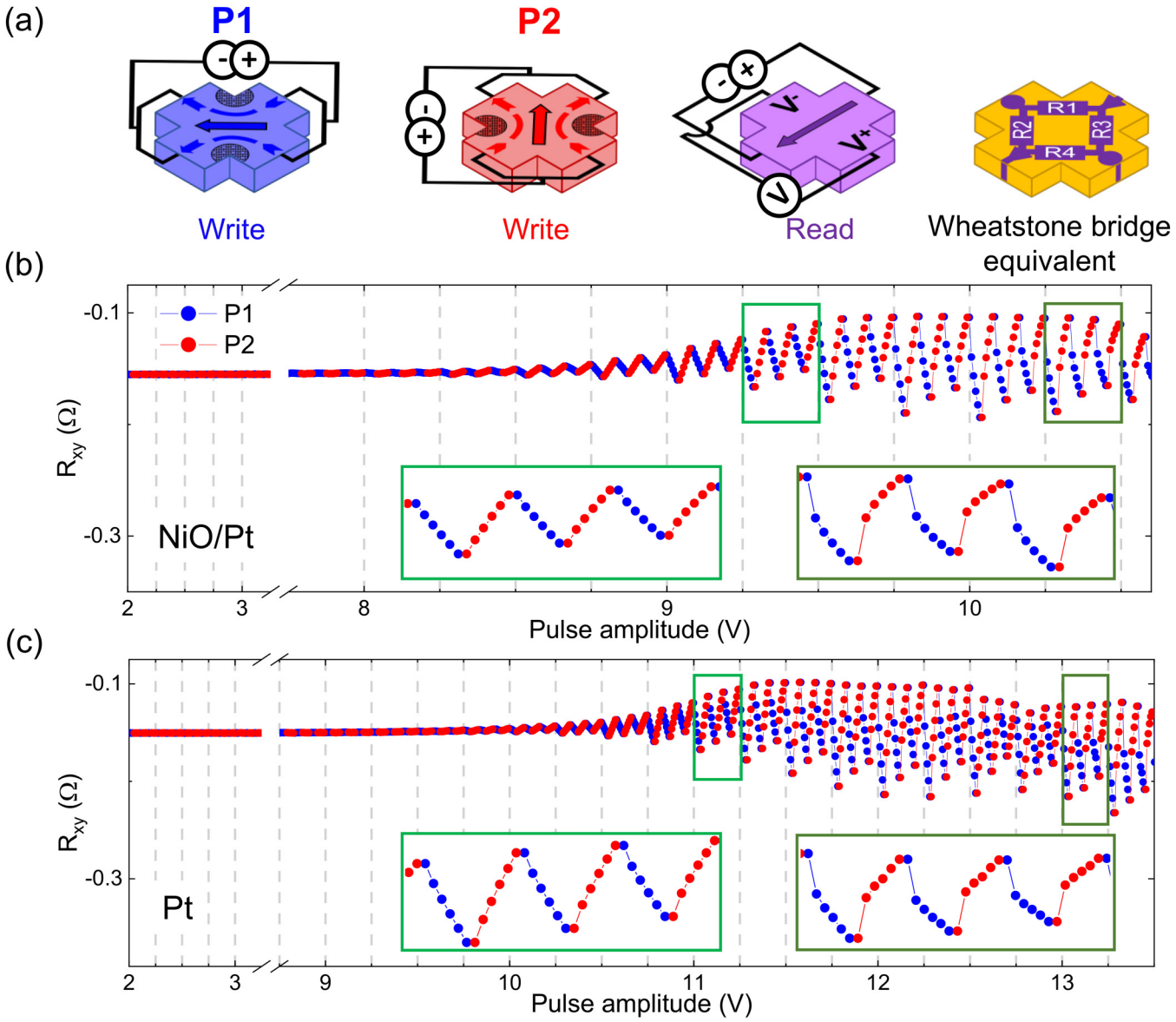

FIG. 1. (a) Illustrative diagrams of the pulsing and reading schemes and the Wheatstone bridge model of a Hall cross with the corresponding resistances R_1, R_2, R_3, and R_4. (b) R_{xy} as a function of writing pulse amplitude measured in Al_2O_3/NiO/Pt and (c) Al_2O_3/Pt 10−μm-wide Hall crosses. The pulse amplitude is increased in steps of 0.25 V in correspondence to the gray dashed lines. For each step, a sequence of three repeats made of five consecutive P1 pulses and five consecutive P2 pulses of length $\tau = 1$ ms is applied. The transverse resistance measured after each pulse is plotted as blue and red dots for P1 and P2 pulses, respectively. The insets show the saw tooth (left) and step-like (right) resistance changes.

arms geometry, even though similar results are obtained on eight-arms crosses.

III. WHEATSTONE BRIDGE MODEL OF A HALL CROSS

According to the considerations presented above, the change in transverse voltage, ΔV_{xy}, due to the switching of antiferromagnetic domains should have opposite sign following the writing pulses P1 and P2. Furthermore, if the switching volume is reversible, the signal should be symmetric in amplitude for P1 and P2 pulses. As shown in this study, however, similar transverse voltage variations to the ones expected for the signature of AFM switching can be observed in Hall crosses due to purely nonmagnetic effects. In order to understand the effects of the pulses onto a nonmagnetic resistive device, it is convenient to model the Hall cross as a Wheatstone bridge. We consider a division of the Hall cross into four quadrants of equal size and corresponding resistances R_1, R_2, R_3, and R_4, as depicted in Fig. 1(a). During pulsing, the current density is higher around the corners due to the current crowding effect.[45] The intense heat generated by the current can affect the metallic structure, which in return would change the resistance of the quadrants: P1 would modify mostly R_1 and R_4, whereas P2 would modify mostly R_2 and R_3. As the sensing current is deflected proportionally to the local resistance, a net voltage arises at the junction of the quadrants, as expected for an unbalanced Wheatstone bridge. For the sensing configuration illustrated in the rightmost panel of Fig. 1(a), the transverse voltage is $V_{xy} = [R_1/(R_1 + R_2) - R_3/(R_3 + R_4)] \cdot V_s$, where V_s is the voltage applied by the sensing current source. The resistances of the arms can be discarded in this model as the arms through which the sensing current flows do not influence the transverse voltage, and there is no current passing through the voltage arms.

The Wheatstone bridge model highlights two important characteristics of the measurement scheme of AFMs in cross-shape devices. First, $V_{xy} = 0$ when $R_1 \cdot R_4 = R_2 \cdot R_3$. Second, and most importantly, the change in transverse voltage consecutive to a pulse, ΔV_{xy}, caused by the variation of R_1 and R_4 has opposite sign than the one caused by the variation of R_2 and R_3. Specifically, ΔV_{xy} is negative for a decrease in R_1 or R_4 but positive for a decrease in R_2 or R_3. Moreover, ΔV_{xy} is positive for an increase in R_1 or R_4 but negative for an increase in R_2 or R_3. This is a crucial point as it shows that a negative ΔV_{xy} after P1 means that the resistance at the corners has decreased relative to the unpulsed state, whereas a positive ΔV_{xy} after P1 means that the resistance has increased. Thus, the sign of ΔV_{xy} allows for discriminating current-induced annealing effects, which tend to reduce the resistance of metal layers, from temporary thermoresistive effects and permanent electromigration effects, which tend to increase the resistance.

IV. DEVICE FABRICATION AND EXPERIMENTAL SETUP

We focus on two different sets of samples: a series of Pt (5nm) reference layers and a series of NiO (10 nm)/Pt (5 nm) bilayers deposited on three different substrates. The numbers between brackets indicate the thickness of each layer. NiO was grown at 550 °C followed by Pt deposition at room temperature after cooling down under vacuum. These layers were sputter-deposited on three different substrates, Si/SiO_2(500 nm), Si/Si_3N_4(400 nm), and sapphire (Al_2O_3), at the same time in order to minimize thickness variations. In these conditions, we obtain a typical roughness of less than 1 nm; all layers are preferentially oriented along the (111)-growth direction. X-ray diffraction measurements indicate a high crystalline epitaxial quality of the NiO layers grown on Al_2O_3, whereas no diffraction peaks are observed for NiO deposited on Si/SiO_2(500 nm) and Si/Si_3N_4(400 nm) for such thickness. A separate batch deposited on Al_2O_3 including a Fe layer on top of NiO confirmed the presence of antiferromagnetic order by means of a reversible exchange bias upon cooling in opposite magnetic fields. All layers were subsequently patterned using reactive ion etching in single and double Hall crosses of different widths from 2.5 μm to 12.5 μm in steps of 0.5 μm. The resistivity of each sample was measured with four point probes in double Hall crosses, giving $\rho_{SiO/Pt} = 3.20 \times 10^{-7}\,\Omega\,m$, $\rho_{SiO/NiO/Pt} = 3.30 \times 10^{-7}\,\Omega\,m$, $\rho_{SiN/Pt} = 3.12 \times 10^{-7}\,\Omega\,m$, $\rho_{SiN/NiO/Pt} = 3.20 \times 10^{-7}\,\Omega\,m$, $\rho_{Al_2O_3/Pt} = 2.38 \times 10^{-7}\,\Omega\,m$, and $\rho_{Al_2O_3/NiO/Pt} = 2.17 \times 10^{-7}\,\Omega\,m$. Although the NiO layer does not significantly affect the Pt resistivity, the high crystalline quality of the NiO and Pt films deposited on Al_2O_3 leads to a lower resistivity than the Si-based substrates. These resistivities are comparable to those obtained for Pt using similar fabrication methods and deposition conditions.[46–48]

The writing pulses were provided by a voltage source that generates rectangular pulses of variable width (50 ns − 1 ms) and amplitude (2 V − 40 V). For instance, a pulse of 10 V corresponds to a current density along the diagonal $j_w = V/(R_p\, t\, \sqrt{2}w) = 0.71 \times 10^{12}\,A/m^2$, where V is the pulse amplitude, $R_p = 200\,\Omega$ is the pulse path resistance measured at the output terminals (typical value), $t = 5$ nm is the film thickness, and $\sqrt{2}w = \sqrt{2} \times 10\,\mu$m is the diagonal of the cross. For reading the transverse voltage, a current source provided an alternating current with a peak-to-peak amplitude of 0.5 mA at a frequency of 10 Hz, corresponding to a current density in the sensing arms of $10^{10}\,A/m^2$ in the same device. The alternating current substantially lowers the noise limit using a pseudo-lock-in detection scheme. The transverse voltage was measured 2 s after pulsing to allow the device to cool down using an integration time of 0.5 s. A relay matrix alternates between the writing (P1 and P2) and the reading configurations. Those relays are essential to control the current path in the device by setting which arms are under tension, floating, or grounded.

V. TRANSVERSE RESISTANCE AS A FUNCTION OF PULSE AMPLITUDE

In most of the reported current-induced switching experiments, the antiferromagnetic materials were epitaxial films. We, thus, first characterize the response of the epitaxial samples $Al_2O_3/NiO/Pt$ and Al_2O_3/Pt. Following the pulse-sense scheme described in Sec. II, Figs. 1(b) and 1(c) illustrate the typical variation of the transverse resistance of $Al_2O_3/NiO/Pt$ and Al_2O_3/Pt 10−μm-wide single Hall crosses following the application of orthogonal pulses P1 and P2. The pulse amplitude is gradually increased in steps of 0.25 V. For each step, a sequence of three repeats, each made of five consecutive P1 pulses followed by five consecutive P2 pulses of length $\tau = 1$ ms, is implemented (delimited by the dashed lines). The transverse resistance measured after

each pulse is plotted as a blue or a red dot for P1 and P2 pulses, respectively. We observe a consecutive decrease and increase in the transverse resistance following P1 and P2 pulses, respectively. The resistance variation increases with the pulse amplitude in both the magnetic and nonmagnetic samples. A change in resistance of $\Delta R_{xy} = 0.05\,\Omega$ is measured for a pulse amplitude of 9.25 V in $Al_2O_3/NiO/Pt$ and 11 V in Al_2O_3/Pt, corresponding to a current density j_w along the diagonal of $0.75 \times 10^{12}\,A/m^2$ and $0.76 \times 10^{12}\,A/m^2$, respectively.

The shape of the signal evolves as the devices undergo several repeats. At first, R_{xy} has a saw-tooth shape as the resistance changes gradually after each of the five consecutive pulses along P1 and P2. At larger voltage, the resistance changes in a step-like manner, where the effect of the first pulse is comparably much larger than the four successive pulses [see insets in Figs. 1(b) and 1(c)]. The saw-tooth shape has been previously associated with resistive changes of the nonmagnetic layer, whereas the step-like shape has been considered as a signature of AFM switching.[17–19,27] This distinction is not supported by the data presented in Fig. 1, in agreement with recent works on magnetic and nonmagnetic samples.[28–30] We also observe a stabilization of the amplitude of the resistance changes after five consecutive pulses with increasing pulse amplitude, which we assign to a training effect. As the behavior of the $Al_2O_3/NiO/Pt$ and Al_2O_3/Pt samples is both qualitatively and quantitatively similar, we attribute the variations of R_{xy} to pulse-induced changes of the Pt resistivity.

The variation in R_{xy} is attributed to the higher current density passing along the corners of the Hall cross [shaded areas in Fig. 1(a)]. According to the Wheatstone bridge model described in Sec. III, the negative and positive ΔR_{xy} after pulsing along P1 and P2, respectively, correspond to a decrease in the local resistivity. These observations indicate that the temperature rise during the pulse anneals the metal layer, which decreases its resistivity after cooling of the device. As the pulse amplitude increases, the annealing process becomes less effective and ΔR_{xy} tends to saturate. This conclusion is corroborated by the work by Wagner *et al.*,[29] in which Nb thin films deposited at room-temperature on an MgO substrate showed a similar decrease in the resistivity along the pulsed-corners of the device. Furthermore, this behavior agrees with previous studies on the resistivity of Pt films, which show an initial decrease followed by an increase in the Pt resistivity as a function of annealing temperature owing to thermally induced redistribution of structural imperfections.[48,49] Finally, measurements performed on $SiO_2/NiO/Pt$, SiO_2/Pt, $Si_3N_4/NiO/Pt$, and Si_3N_4/Pt all show a similar behavior with no systematic differences between them that could evidence a magnetic signal.

In the literature, the nonmagnetic variation of R_{xy} in AFM/Pt bilayers has been assigned to two other effects. One is the temporary increase in local resistivity due to Joule heating that persists during sensing.[30] The other is electromigration occurring at the corners of the Hall cross, which causes the formation of hillocks and metal voids that increase the local resistivity.[29,30] Both these effects would result in ΔR_{xy} of opposite sign with respect to our measurements. Concerning the first effect, the waiting time between the writing and reading events is about 2 s, which is long enough for the device to thermalize to the substrate temperature.[50,51] As for electromigration, we cannot exclude that it coexists with thermal annealing. Likely, however, electromigration dominates at voltages higher than 20 V in our 10−μm-wide Hall crosses ($j_w > 1.7 \times 10^{12}\,A/m^2$), as we also observe an increase in the resistance preceding the device breakdown at high current density (see Sec. IX). Other models have linked ΔR_{xy} to a Seebeck voltage along the direction of the current-induced temperature gradient in Pt.[28] Accordingly, if the Seebeck voltage is at the origin of the change in the transverse resistance, the measured voltage should be independent of the sensing current. Contrary to this hypothesis, we find a linear relationship between ΔV_{xy} and the sensing current between 0.1 mA and 10 mA, which confirms the resistive origin of ΔR_{xy}.

VI. TEMPORAL RELAXATION OF THE TRANSVERSE RESISTANCE AFTER PULSING

After pulsing, R_{xy} relaxes toward the pre-pulse value on a time-scale of hours. Figure 2 illustrates the typical evolution of R_{xy} over 2 h following single pulses P1 (blue) and P2 (red) in $Al_2O_3/NiO/Pt$ and Al_2O_3/Pt. The timing of the single pulses is denoted by dashed lines. As a reference, R_{xy} of the pristine device is recorded starting 1 h before the first pulse P1 to demonstrate the absence of drift in the measurements. The relaxation, which we observe in nonmagnetic and magnetic samples alike, is characterized by different short and long time scales that cannot be captured by a simple exponential fit. To fit the data, we, thus, use a double exponential function $R_{xy}(t) = y_0 + A_1 \cdot \exp(-(t - t_0)/\lambda_1) + A_2 \cdot \exp(-(t - t_0)/\lambda_2)$, where $t_0 = 2$ s is the time interval between the pulse and the sense current, $A_{1,2}$ are amplitude parameters, and $\lambda_{1,2}$ are the relaxation times. Such double exponential decay is typical of relaxation processes in metallic glasses, where the fast process is local and reversible and the slow one involves large scale irreversible structural rearrangements due to the subdiffusive motion of atoms.[52,53]

The fits of P1 and P2 curves (black lines in Fig. 2) give a short decay time of $\lambda_1 = 4 \pm 0.6$ min and 4.2 ± 0.2 min for $Al_2O_3/NiO/Pt$ and Al_2O_3/Pt, respectively, and a long decay time of $\lambda_2 = 48 \pm 5$ min and 56 ± 3 min. These short and long decay times are of the same order of magnitude in the six different samples considered in this study. Also, we find that the fit coefficients do not depend significantly on the substrate or the presence of the NiO layer. A similar relaxation process was observed in MgO/Pt, Si/Pt and glass/Pt[28] but was attributed to slow cooling through the substrate and a long lasting transverse voltage due to the Seebeck effect across the device. This interpretation, however, requires the amplitude of the transverse voltage to be independent of the sensing current, which is not compatible with the linear relation between the transverse voltage and the sensing current found in our measurements (see Sec. V). Other studies of Pt and NiO/Pt have related the long lasting relaxation of R_{xy} to the diffusional creep induced by electromigration with the Pt grain boundaries acting as sources and sinks for point defects.[30]

We further note that the long lasting relaxation process is not observed in the consecutive pulse-sense-pulse measurements reported in Figs. 1(b) and 1(c) as the time interval between these steps is too short (about 2 s). However, in such consecutive measurements, the relaxation manifests itself as a drift of the resistance baseline. Moreover, the relaxation can induce a sign inversion of

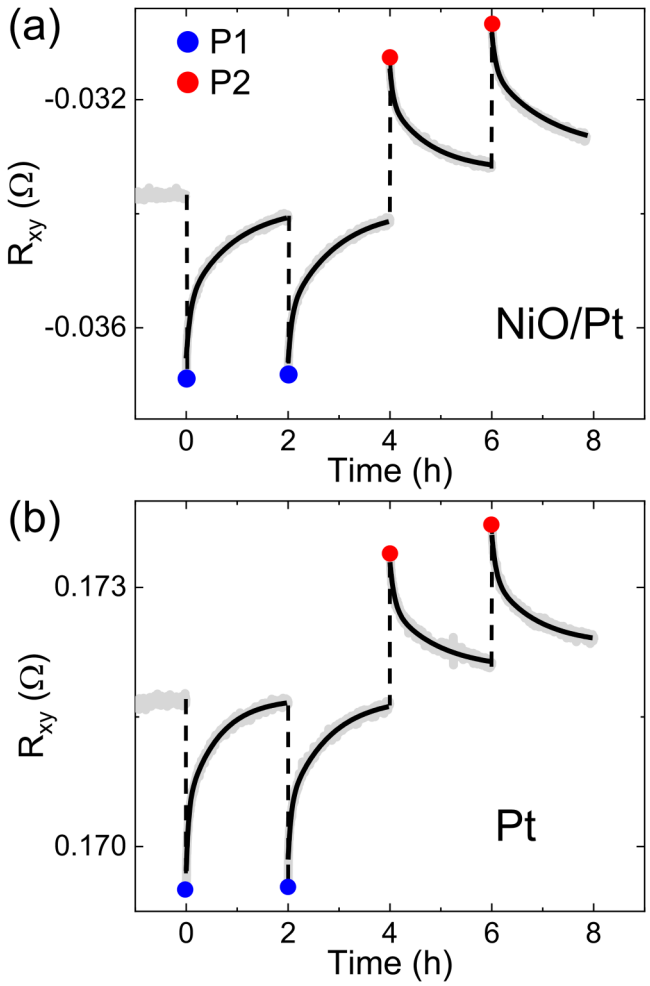

FIG. 2. Relaxation of the transverse resistance following single pulses P1 (blue dots) and P2 (red dots) for Al_2O_3/NiO/Pt (a) and Al_2O_3/Pt (b) in 10-μm-wide Hall crosses. The timing of each pulse is indicated by a vertical dashed line. The solid black lines are fits with a double exponential function (see text for details).

ΔR_{xy} in consecutive pulse-sense-pulse measurements, which we discuss in Sec. VII.

VII. TRANSVERSE RESISTANCE AS A FUNCTION OF PULSE AMPLITUDE AND PULSE LENGTH

In this section, we analyze the response of the devices when the length of the writing pulses is reduced from 1 ms to below 1 μs. Following the same procedure described in Sec. V, Figs. 3(a)–3(c) show the change of R_{xy} in a Al_2O_3/Pt 10 − μm-wide Hall cross as a function of pulse amplitude for pulse lengths of 1 ms, 14 μs, and 850 ns. In order to avoid extensive training and break down of the devices during the measurements, the pulse amplitude is increased in steps of 0.25 V until $\overline{\Delta R_{xy}} \geq 0.01\,\Omega$, where $\overline{\Delta R_{xy}}$ is the arithmetic mean of the change in resistance after five pulses over the three repeats that are recorded at the same pulse amplitude. Figures 3(d)–3(f) report $\overline{\Delta R_{xy}}$ calculated from the traces in Figs. 3(a)–3(c). We observe that the minimum pulse amplitude required to obtain a noticeable $\overline{\Delta R_{xy}} \geq 0.001\,\Omega$ increases systematically for shorter pulses: 10.5 V, 11 V, and 20 V for a pulse length of 1 ms, 14 μs, and 850 ns, respectively. This highly nonlinear relation between the pulse amplitude and the pulse length suggests an interplay between the current-induced Joule heating of the device and heat dissipation through the substrate. Such behavior is expected if $\overline{\Delta R_{xy}}$ is due to current-induced annealing, as the probability of thermally activated processes depends linearly on time and exponentially on the inverse of the temperature.

The curves shown in Fig. 3 evidence also a variation of the baseline of R_{xy}, which changes from straight in (a) to nonmonotonic in (b) and (c). This effect is ascribed to the training of the device. In a pristine device, as the voltage is ramped up for the first time, R_{xy} decreases after P1 pulses and comes back to its previous value after an equal number of P2 pulses, as shown in Fig. 3(a). As the ramp in Fig. 3(a) ends with five pulses along P2, R_{xy} is large and tends to relax at the beginning of the second ramp, shown in Fig. 3(b). Depending on the length, spacing, and amplitude of the pulses, the interplay of excitation and relaxation effects results in a changing baseline of R_{xy}, as discussed in more detail in Sec. X.

Measurements performed with shorter pulses evidence an another remarkable effect, namely, the inversion of the sign of ΔR_{xy} preceding the onset of the larger variations of ΔR_{xy}, which can be observed in the inset of Fig. 3(c). The sign inversion becomes more clear when plotting $\overline{\Delta R_{xy}}$, namely, the average excursion of the trace as a function of the pulse amplitude. At high voltage, $\overline{\Delta R_{xy}}$ is consistent with a decrease in R_{xy} induced by pulsing, as described in Sec. V. At an intermediate amplitude, however, the sign of $\overline{\Delta R_{xy}}$ is inverted, as seen by the difference of the blue and red curves in Fig. 3(f) and in the inset of Fig. 3(c). The sign inversion typically appears when multiple pulses are applied to Pt and NiO/Pt devices and when the training state is more advanced.

We assign this transient sign inversion to heat-assisted relaxation induced by a current pulse, which can dominate over annealing in trained devices. During the first ramp, each pair of the device quadrants, $R_{1,4}$ and $R_{2,3}$ (see Sec. III), undergoes the same annealing effect and ΔR_{xy} for P1 (P2) is successively negative (positive). Then, in the small amplitude regime at the beginning of the following ramps, the four quadrants uniformly relax and give $\Delta R_{xy} \approx 0$. Upon increasing the pulse amplitude, the temperature of the quadrants gradually rises, which speeds up the relaxation of these quadrants compared to the unpulsed quadrants. This asymmetric change of resistance induces a positive (negative) ΔR_{xy} after P1 (P2) pulses. This transient state takes place only in a small range of pulse amplitudes, namely, when the current supplies enough heat to accelerate the relaxation rate without initiating the annealing process. The amplitude of this effect depends on the training history of the sample and changes from device to device.

VIII. INFLUENCE OF THE ANTIFERROMAGNETIC LAYER AND SUBSTRATE

In order to investigate the influence of the NiO layer and of the substrate on the transverse resistance, we compare the average

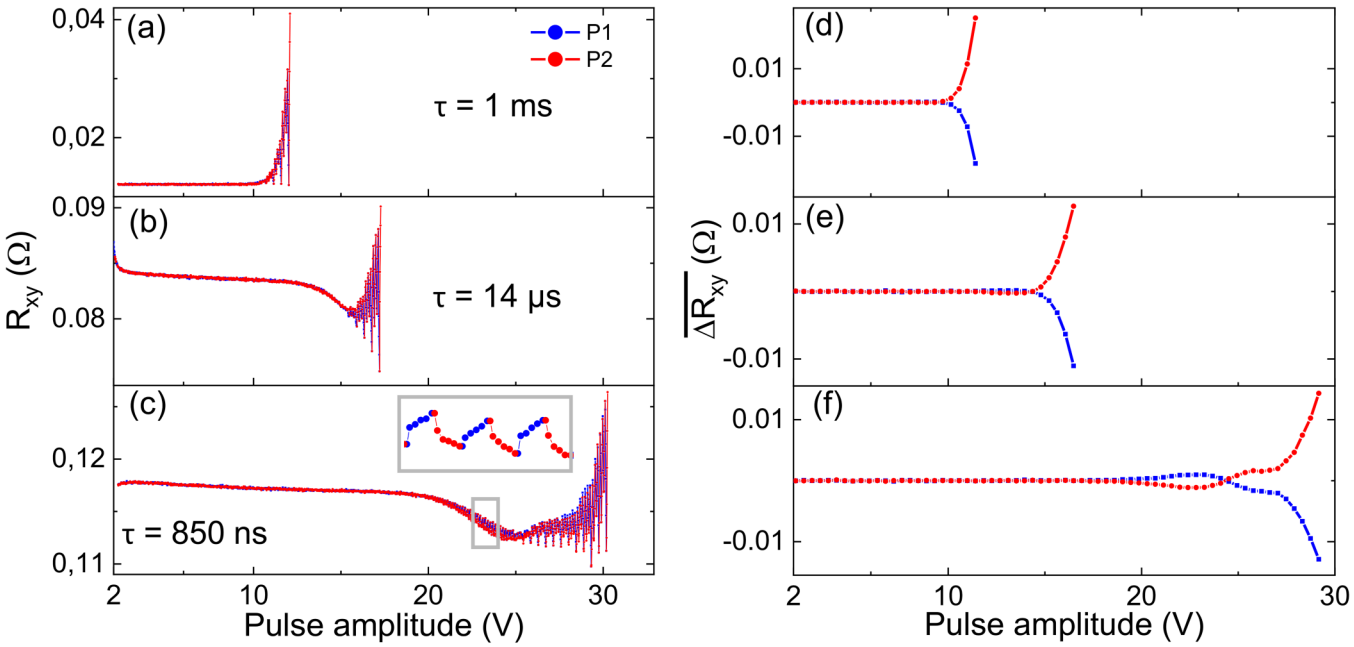

FIG. 3. (a)–(c) R_{xy} as a function of writing pulse amplitude measured in a Al_2O_3/Pt 10 − μm-wide Hall cross for pulses of length (a) 1 ms, (b) 14 μs, and (c) 850 ns. The pulse amplitude is increased in steps of 0.25 V. For each step, a sequence of three repeats of five consecutive P1 pulses and five consecutive P2 pulses is applied, as in Figs. 1(b) and 1(c). (d)–(f) $\overline{\Delta R_{xy}}$ is the average change of resistance after five pulses calculated over three repeats at constant pulse amplitude from the traces in (a)–(c). The pulsing ramps were stopped when $\overline{\Delta R_{xy}} \geq 0.01\,\Omega$. The inset shows the R_{xy} trace with an inverted sign change.

$\overline{\Delta R_{xy}}$ as a function of the pulse amplitude and pulse length for Pt and NiO/Pt deposited on Si/SiO_2, Si/Si_3N_4, and Al_2O_3, as shown in Fig. 4(a)–4(f). In these plots, the colors represent the amplitude of $\overline{\Delta R_{xy}}$ measured after P1 pulses and the gray areas represent the range where $\overline{\Delta R_{xy}} \approx 0$. No measurements were acquired in the white areas because the change in resistance exceeded the limit of $\overline{\Delta R_{xy}} \geq 0.01\,\Omega$. The measurements of $\overline{\Delta R_{xy}}$ recorded after P2 pulses are roughly symmetric and opposite in sign to P1, corresponding to complementary color maps with inverted blue and red colors.

We find that the presence of NiO makes very little difference in the response of the devices. Neither the NiO/Pt sample with high epitaxial quality grown on Al_2O_3 nor those grown on SiO_2 and Si_3N_4 show significant differences with respect to the single Pt layers, confirming that the resistance variation in such structures originates from Pt rather than from switching of the AFM.

In all devices, the pulse amplitude required to attain a given variation of R_{xy} increases as the pulse length is reduced. However, the rate at which $\overline{\Delta R_{xy}}$ rises as a function of pulse amplitude and pulse length is closely related to the substrate. In order to maintain the same $\overline{\Delta R_{xy}}$ amplitude when reducing the pulse length by a factor 1000, the pulse amplitude needs to be increased by a factor 2 for the samples grown on SiO_2 and Si_3N_4 and by a factor of 3 for the samples grown on Al_2O_3. This observation can be rationalized in terms of thermal diffusivity $\mu_s = \kappa_s/(\rho_s c_s)$ of the substrate, which exemplifies how well a material conducts heat in terms of thermal conductivity κ_s relative to its volumetric capacity for storing thermal energy, as given by the product of density ρ_s and specific heat c_s. At room temperature, the thermal diffusivity calculated from thin film parameters is $\mu_{SiO_2} \approx 0.8\,mm^2\,s^{-1}$ for SiO_2 ($\kappa = 1.3\,W\,m^{-1}\,K^{-1}$, $\rho = 2200\,kg\,m^{-3}$, and $c = 730\,J\,kg^{-1}\,K^{-1}$), $\mu_{Si_3N_4} \approx 0.9\,mm^2\,s^{-1}$ for Si_3N_4 ($\kappa = 1.4\,W\,m^{-1}\,K^{-1}$, $\rho = 2100\,kg\,m^{-3}$, and $c = 730\,J\,kg^{-1}\,K^{-1}$[50,54]), and from bulk parameters $\mu_{Al_2O_3} \approx 28\,mm^2\,s^{-1}$ for Al_2O_3 ($\kappa = 46.06\,W\,m^{-1}\,K^{-1}$, $\rho = 3980\,kg\,m^{-3}$, and $c = 418\,J\,kg^{-1}\,K^{-1}$[55]). The gray shaded areas in Fig. 4 show that the substrates with high thermal diffusivity allow for using a larger range of pulse amplitudes and pulse lengths without inducing changes of R_{xy}. This finding is explained by the fact that substrates with a large thermal diffusivity can transfer heat fast without heating up too much compared to substrates with a low thermal diffusivity.

As a corollary, we note that the heat effectively dissipated in Pt depends on the balance between electrical power supplied to the system, heat transfer by conduction through the NiO and the substrate, and convection and radiation at the top of the devices. However, the convective and radiation heat losses are much smaller than the conduction heat transfer[56] and roughly equal for all the devices investigated in this study. Therefore, we conclude that the thermal diffusivity of the substrate is the main parameter affecting the heat accumulation in Pt induced by a given current in devices of equal size.

The temperature increase attained during the pulse is related to the electrical energy dissipated in the device, $E = \tau V^2/R_p$, where τ is the pulse length, R_p is the resistance of the pulse path, and V is the applied voltage. Figure 5 plots the energy required to induce a

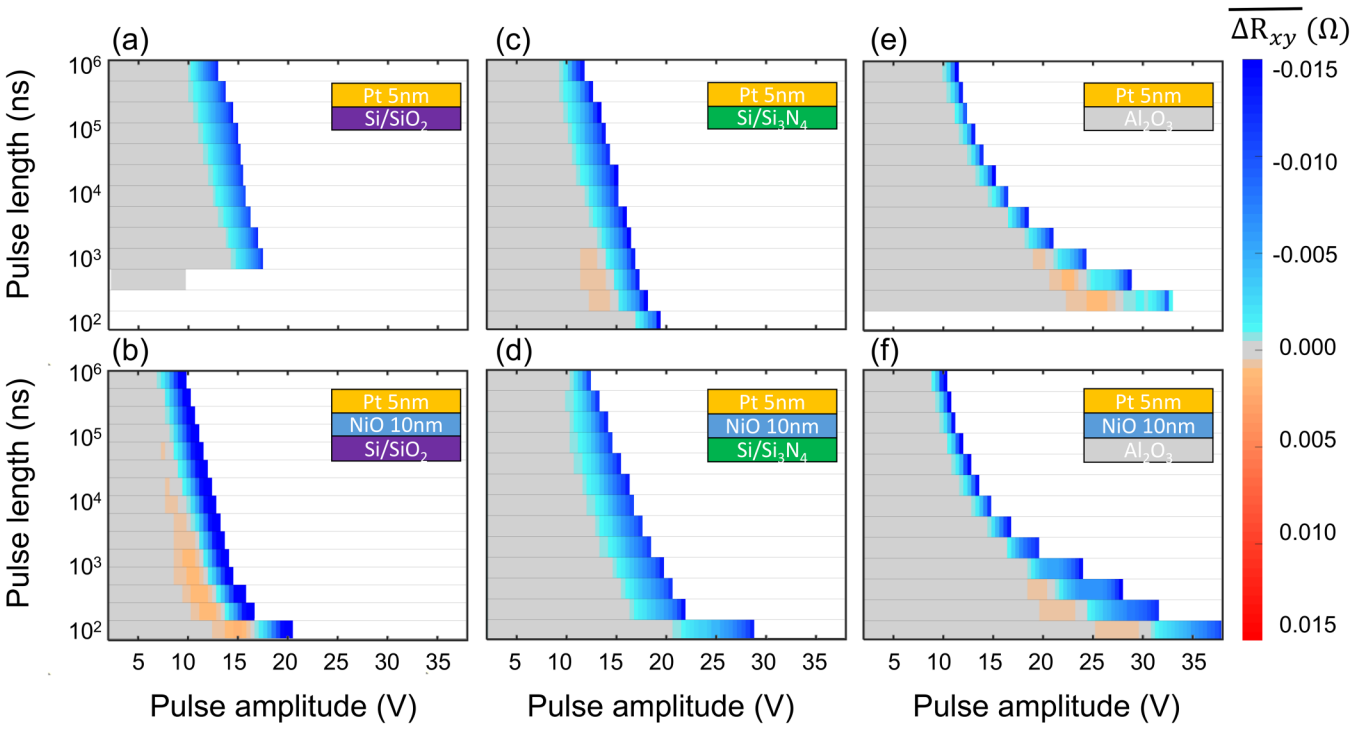

FIG. 4. Comparison of the average transverse resistance change as a function of pulse amplitude and pulse length in a 10-μm-wide Hall cross of (a) SiO_2/Pt, (b) SiO_2/NiO/Pt, (c) Si_3N_4/Pt, (d) Si_3N_4/NiO/Pt, (e) Al_2O_3/Pt, and (f) Al_2O_3/NiO/Pt. The plots show $\overline{\Delta R_{xy}}$ measured after five consecutive P1 pulses and averaged over three repeats at the constant pulse amplitude following the same measurement scheme reported in Fig. 3. For each pulse length, a ramp of increasing pulse amplitude is applied until $\overline{\Delta R_{xy}} \geq 0.01\Omega$. The color scale represents the amplitude and sign of $\overline{\Delta R_{xy}}$. Gray-shaded areas indicate no resistance change.

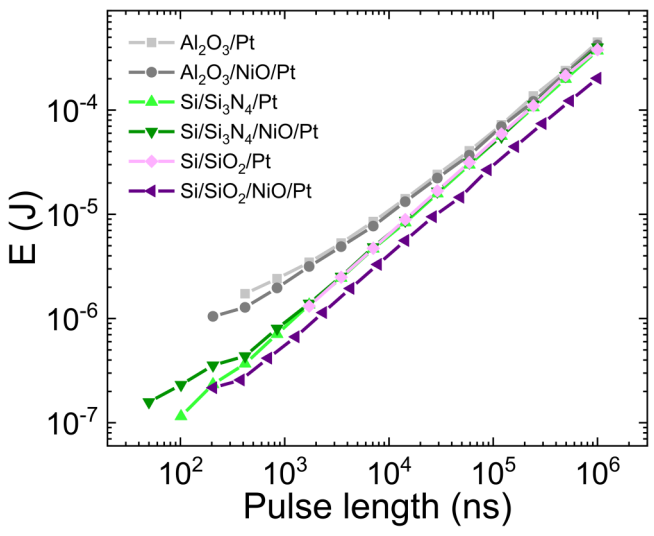

FIG. 5. Electrical energy $E = \tau V^2/R_p$ required to obtain a relative change of the transverse resistance $\overline{\Delta R_{xy}}/\Delta R_{xx} \geq 10^{-5}$ as a function of pulse length computed from the data in Fig. 4.

relative change $\overline{\Delta R_{xy}}/R_{xx} \geq 10^{-5}$ as a function of pulse length. The curves confirm that samples grown on SiO_2 and Si_3N_4 substrates require less energy compared to Al_2O_3 in order to attain a similar change in resistance. Moreover, when comparing the Al_2O_3 and Si-based substrates, the curves follow the same trend for long pulses but diverge for short pulses, showing that the samples grown on Al_2O_3 dissipate heat more efficiently for shorter pulses compared to longer pulses. We attribute this trend to the timescale required to transfer heat from the device to the substrate. For short pulses, $\tau \leq 10\,\mu$s, the temperature rises sharply in the device but not in the substrate. For longer pulses, on the other hand, the heat dissipated in the device diffuses to the substrate and warms it up. The heat diffusivity of the Si-based substrates varies little with increasing temperature,[54,57] whereas the heat diffusivity of Al_2O_3 drops from $\sim 28\,mm^2\,s^{-1}$ at room temperature to $\sim 15\,mm^2\,s^{-1}$ at 100 °C, and $\sim 8\,mm^2\,s^{-1}$ at 400 °C.[55] Therefore, Al_2O_3 becomes significantly less efficient in dissipating heat for the longer pulses, which explains the converging trend of the curves shown in Fig. 5.

IX. SIZE EFFECTS

The power density dissipated in Pt is given by $V^2/(\rho L^2)$, where L is the effective length of the pulse path, which is approximately independent of the device width. As the current distribution

in the Hall cross is inhomogeneous, however, we find that the device width strongly influences the amplitude of ΔR_{xy}. More precisely, we observe that ΔR_{xy} increases as the ratio between the area of the Hall cross and the length of the excited path decreases. Figure 6(a) reports ΔR_{xy} as a function of pulse amplitude for Si_3N_4/Pt Hall crosses with width ranging from 2.5 μm to 12.5 μm in steps of 2.5 μm. To study the asymmetry induced by the writing current, only the top right quadrant of the device is pulsed, exciting mainly R_1 (see Sec. III), in sequences of 10 pulse-repeats starting from 2 V and increasing in steps of 0.25 V until the device fails.

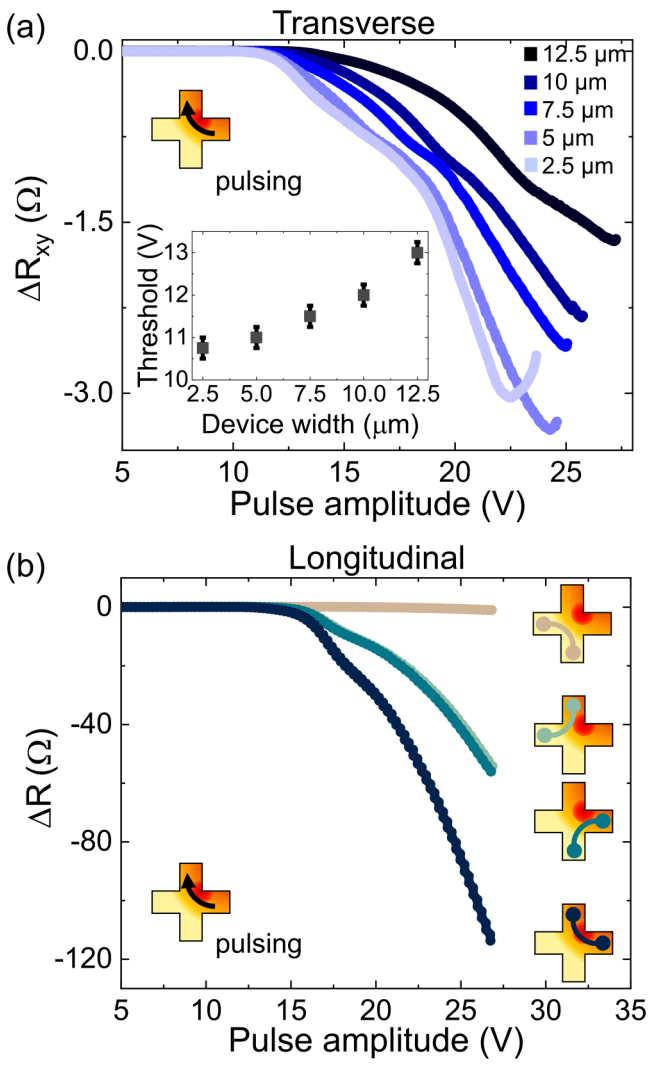

FIG. 6. (a) Change in the transverse resistance ΔR_{xy} as a function of pulse amplitude for pulses sent around one corner of a Hall cross (see arrow). The data are measured in Si_3N_4/Pt(5 nm) Hall crosses of different widths. (b) Change of the longitudinal resistance ΔR of the four quadrant paths of a 5-μm-wide cross as a function of pulse amplitude for pulses sent around one corner of the cross. The pulsing and measuring geometry are indicated in the schematic diagrams. The initial resistance of each path is, on average, $R_0 = 703 \pm 1\,\Omega$.

We observe that ΔR_{xy} is negative and decreases markedly up to a pulse amplitude of about 25 V, after which it starts increasing just before reaching the device breakdown. As argued in Sec. V, the decrease in R_{xy} in this geometry corresponds to a decrease in the local resistivity, whereas the final upturn corresponds to an increase in the local resistivity. These measurements support the conclusion that competing effects take place in the crosses, consistently with thermal annealing and electromigration dominating the intermediate and higher voltage range, respectively. Importantly, smaller crosses present larger ΔR_{xy} signals compared to larger crosses. The inset in Fig. 6(a) shows that the pulse amplitude threshold for observing $\Delta R_{xy} \geq 0.01\,\Omega$ increases with the width of the cross, which we attribute to the larger proportion between the device area and the current-crowded area.

The variation of the longitudinal resistance ΔR measured between two adjacent arms of the cross, shown in Fig. 6(b), is consistent with the decrease in R_{xy} derived from the Wheatstone model. Moreover, we observe that the resistance change not only occurs at the corresponding corner where the current density is the highest, but also in its surroundings and the pulsed arms. Before the breakdown of the device, the maximum relative change of the longitudinal resistance is $\Delta R/R \approx -16\%$ measured along the pulse path (black curve), $\approx -8\%$ in the two adjacent quadrant paths (light and dark green curves), and $\approx -0.14\%$ in the quadrant opposite to the pulse path (orange curve).

X. INFLUENCE OF TRAINING EFFECTS ON THE RESISTANCE BASELINE

In this section, we analyze the nonlinear variation of the baseline of R_{xy} as a function of the pulse amplitude, which determines the shape of the traces shown in Figs. 1(b), 1(c), and 3(a)–3(c). We argue that this shape is due to training of the devices. To understand the effects of training, we first measure R_{xy} after pulsing the device only along P1, as shown in Fig. 7(a), then only along P2, as shown in Fig. 7(b), and finally run the sequence of alternate P1 and P2 pulses already described in Sec. V, as shown in Fig. 7(c). The ramps shown in Figs. 7(a)–7(c) are taken consecutively with no waiting time between each other. During the first ramp, R_{xy} progressively decreases with the increasing number of P1 pulses. The signal of the second ramp starts from the value of R_{xy} attained at the end of the first ramp and varies in the opposite direction with an increasing number of P2 pulses. We note that here the relaxation process (Fig. 2) is not visible because of the short period of time elapsed during the ramp. By overlapping the first and second ramps [black dashed line and red line in Fig. 7(b)], we observe that the end value of R_{xy} in the P2 ramp is smaller by about $\approx 20\%$ compared to the P1 ramp. This asymmetry between the P1 and P2 responses is attributed to the training of the device during the first ramp, as P1 pulses also partially affect the resistance of the P2 pulse path (see Fig. 6). This interpretation was confirmed by inverting the order of the pulses, namely, when the P2 ramp preceded the P1 ramp in a pristine device, which led to the opposite asymmetry. Thus, the amplitude of ΔR_{xy} following P1 and P2 pulses

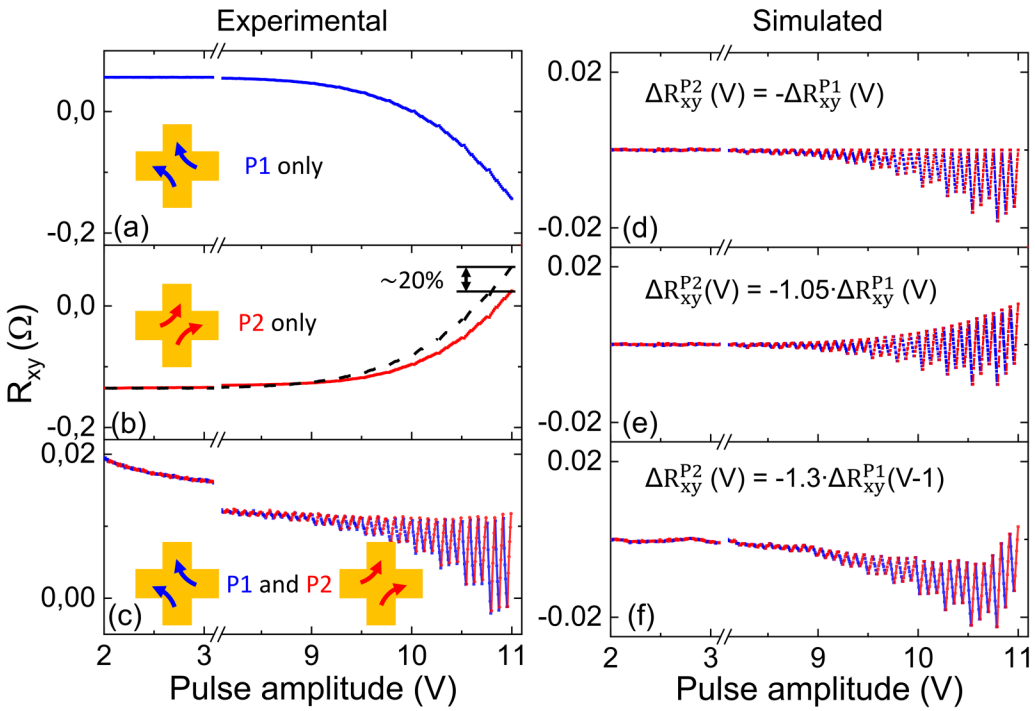

FIG. 7. Variation of R_{xy} in a 10-μm-wide Si_3N_4/Pt cross as a function of pulse amplitude for P1 (a), P2 (b), and P1 and P2 pulses (c). In each ramp, the pulse amplitude is increased in steps of 0.25 V. For each step, a sequence of three repeats of five consecutive P1 or P2 pulses of length $\tau = 1$ ms is applied. (d) Simulated device response to P1 and P2 pulsing calculated from the curves shown in (a) and (b) by assuming a symmetric response along P1 and P2, $[\Delta R_{xy}^{P2}(V) = -\Delta R_{xy}^{P1}(V)]$, (e) a 5% higher ΔR_{xy} for P2 pulses, $[\Delta R_{xy}^{P2}(V) = -1.05 \cdot \Delta R_{xy}^{P1}(V)]$, and (f) a 30% higher amplitude and a 1 V shift of the threshold for P2 pulses, $[\Delta R_{xy}^{P2}(V) = -1.3 \cdot \Delta R_{xy}^{P1}(V-1)]$.

depends on the pulsing history as well as from possible structural imperfections in the Hall cross due to inhomogeneous growth or patterning.

When considering a ramp of alternating P1 and P2 pulses, the asymmetry of ΔR_{xy} between P1 and P2 pulses results in a nonmonotonic baseline of R_{xy} that can be mistaken for drift but is actually the signature of unequal responses to P1 and P2 pulses. In Fig. 7(c), as the same number of pulses have been applied to the four corners in (a) and (b), the resistance changes along the paths of P1 and P2 are partially balanced. Hence, the ramp with alternate pulses along P1 and P2 is close to symmetric. In general, however, the device never goes back to a fully balanced state after pulsing along P1 and P2, giving rise to different baseline shapes, as observed, e.g., in Figs. 1(b), 1(c), and 3(a)–3(c). To see how this occurs in practice, we have simulated the P1 and P2 pulsing ramps starting from the curves shown in Figs. 7(a) and 7(b), computing the sum of the points measured along P1 and P2 (alternating five P1 pulses and five P2 pulses), and artificially removing or introducing asymmetries in response to P2 pulses $[\Delta R_{xy}^{P2}(V)]$ relative to P1 $[\Delta R_{xy}^{P1}(V)]$. The results are shown in Figs. 7(d)–7(f), where we reproduce different baselines by assuming [Fig. 7(d)] a symmetric response with $\Delta R_{xy}^{P2}(V) = -\Delta R_{xy}^{P1}(V)$, [Fig. 7(e)] a 5% higher response along P2, $\Delta R_{xy}^{P2}(V) = -1.05 \cdot \Delta R_{xy}^{P1}(V)$, and [Fig. 7(f)] an asymmetric response of the device along P2 by shifting the voltage axis by 1 V and increasing the amplitude of the response by 30% such that $R_{xy}^{P2}(V) = -1.3 \cdot \Delta R_{xy}^{P1}(V-1)$. In agreement with the experiments, we see that the resistance change can take three forms: the baseline of ΔR_{xy} can stay constant at the first value of the series with R_{xy} moving back and forth with pulses along P1 and P2 [Fig. 7(d)], tilt upward or downward [Fig. 7(e)], or describe a nonmonotonic curve similar to a "pipe" [Fig. 7(f)].

Interestingly, the shape of R_{xy} reported in Fig. 7(e) can be misinterpreted as a symmetric response to P1 and P2 pulses because the excursion of R_{xy} appears to be symmetric around a central value. However, a symmetric response implies the ability to return always to the initial value of R_{xy}, as shown in Fig. 7(d). More complex shapes are obtained when there is an asymmetry in both the amplitude response and threshold voltage required to induce appreciable changes of R_{xy}, as shown in Fig. 7(f). Note that in Ref. 13, a similar shape as the one reported in Fig. 7(f) has been associated with a partial reorientation of the Néel vector in an antiferromagnetic transition metal dichalcogenide. However, we repeatedly observed this behavior in Pt samples and in NiO/Pt bilayers [see Fig. 7(c)], which shows that special care should be taken when analyzing the signal trace in such a device geometry and pulsing configuration.

XI. CONCLUSIONS

In conclusion, we presented a comparative analysis of the current-induced resistance variation in Pt and NiO/Pt samples. A systematic study of the pulse amplitude and pulse length dependence of the transverse resistance performed on epitaxial and non-epitaxial films did not evidence significant differences between Pt and NiO/Pt layers. All our results are consistent with changes in the Pt resistivity occurring at the corners of the Hall crosses due to the current crowding effect. As also seen in recent works,[28–30] the resistance can change in a saw tooth or step-like manner in both magnetic and nonmagnetic samples, and therefore, the signal shape cannot be used to unambiguously identify magnetic switching, even if *ex situ* imaging confirms the reversal of antiferromagnetic domains.[17–19,27] Using a simple Wheatstone bridge model of a Hall cross, we identified competing effects responsible for the resistance changes: a decrease in local resistivity surrounding the pulsed corner due to thermal annealing of the Pt layer and an increase in the resistivity due to electromigration preceding the device breakdown. After pulsing, the transverse resistance relaxes back toward the value before the pulse following a double exponential law with a short and long relaxation time of about a few minutes and 1 h, respectively. The interplay between the voltage amplitude and relaxation can give rise to nonmonotonic changes and even sign inversion of the variation of resistance. The substrate, apart from determining the crystalline quality of the samples, plays an essential role in dissipating heat away from the Pt line during pulsing. Substrates with a large thermal diffusivity such as sapphire allow for using a significantly broader range of pulse amplitudes without causing changes in the resistance due to current-induced annealing of Pt, thus providing a better chance of measuring magnetic switching by electrical means without artifacts. At constant pulse amplitude, larger devices show reduced resistance changes compared to smaller devices owing to the larger proportion between the device area and the current-crowded area. Finally, we find that the current-induced changes of the transverse resistance are superimposed onto a nonmonotonic baseline whose shape depends on structural imperfections and device asymmetry as well as on the pulsing history of the sample. Our results provide a systematic overview of current-induced resistance changes in single metal layers and antiferromagnet/metal bilayers. These signals have a nonmagnetic origin and might either obscure or overlap with the magnetoresistive signals due to the switching of antiferromagnetic domains in antiferromagnet/metal bilayers.

ACKNOWLEDGMENTS

This work was funded by the Swiss National Science Foundation (Grant No. PZ00P2-179944).

DATA AVAILABILITY

The data that support the findings of this study are available from the corresponding author upon reasonable request.

REFERENCES

[1]K. Olejník, V. Schuler, X. Marti, V. Novák, Z. Kašpar, P. Wadley, R. P. Campion, K. W. Edmonds, B. L. Gallagher, J. Garces, M. Baumgartner, P. Gambardella, and T. Jungwirth, "Antiferromagnetic CuMnAs multi-level memory cell with microelectronic compatibility," Nat. Commun. **8**, 15434 (2017).
[2]T. Jungwirth, X. Marti, P. Wadley, and J. Wunderlich, "Antiferromagnetic spintronics," Nat. Nanotechnol. **11**, 231–241 (2016).
[3]F. Keffer and C. Kittel, "Theory of antiferromagnetic resonance," Phys. Rev. **85**, 329–337 (1952).
[4]M. Fiebig, N. P. Duong, T. Satoh, B. B. Van Aken, K. Miyano, Y. Tomioka, and Y. Tokura, "Ultrafast magnetization dynamics of antiferromagnetic compounds," J. Phys. D Appl. Phys. **41**, 164005 (2008).
[5]V. Baltz, A. Manchon, M. Tsoi, T. Moriyama, T. Ono, and Y. Tserkovnyak, "Antiferromagnetic spintronics," Rev. Mod. Phys. **90**, 015005 (2018).
[6]K. Olejník, T. Seifert, Z. Kašpar, V. Novák, P. Wadley, R. P. Campion, M. Baumgartner, P. Gambardella, P. Němec, J. Wunderlich, J. Sinova, P. Kužel, M. Müller, T. Kampfrath, and T. Jungwirth, "Terahertz electrical writing speed in an antiferromagnetic memory," Sci. Adv. **4**, eaar3566 (2018).
[7]P. Wadley, B. Howells, J. Elezny, C. Andrews, V. Hills, R. P. Campion, V. Novak, K. Olejnik, F. Maccherozzi, S. S. Dhesi, S. Y. Martin, T. Wagner, J. Wunderlich, F. Freimuth, Y. Mokrousov, J. Kune, J. S. Chauhan, M. J. Grzybowski, A. W. Rushforth, K. W. Edmonds, B. L. Gallagher, and T. Jungwirth, "Electrical switching of an antiferromagnet," Science **351**, 587–590 (2016).
[8]P. Wadley, S. Reimers, M. J. Grzybowski, C. Andrews, M. Wang, J. S. Chauhan, B. L. Gallagher, R. P. Campion, K. W. Edmonds, S. S. Dhesi, F. Maccherozzi, V. Novak, J. Wunderlich, and T. Jungwirth, "Current polarity-dependent manipulation of antiferromagnetic domains," Nat. Nanotechnol. **13**, 362–365 (2018).
[9]X. F. Zhou, J. Zhang, F. Li, X. Z. Chen, G. Y. Shi, Y. Z. Tan, Y. D. Gu, M. S. Saleem, H. Q. Wu, F. Pan, and C. Song, "Strong orientation-dependent spin–orbit torque in thin films of the antiferromagnet Mn_2Au," Phys. Rev. Appl. **9**, 054028 (2018).
[10]M. Meinert, D. Graulich, and T. Matalla-Wagner, "Electrical switching of antiferromagnetic Mn_2Au and the role of thermal activation," Phys. Rev. Appl. **9**, 064040 (2018).
[11]S. Y. Bodnar, L. Šmejkal, I. Turek, T. Jungwirth, O. Gomonay, J. Sinova, A. A. Sapozhnik, H.-J. Elmers, M. Kläui, and M. Jourdan, "Writing and reading antiferromagnetic Mn_2Au by Néel spin–orbit torques and large anisotropic magnetoresistance," Nat. Commun. **9**, 348 (2018).
[12]X. Chen, X. Zhou, R. Cheng, C. Song, J. Zhang, Y. Wu, Y. Ba, H. Li, Y. Sun, Y. You, Y. Zhao, and F. Pan, "Electric field control of Néel spin–orbit torque in an antiferromagnet," Nat. Mater. **18**, 931–935 (2019).
[13]N. L. Nair, E. Maniv, C. John, S. Doyle, J. Orenstein, and J. G. Analytis, "Electrical switching in a magnetically intercalated transition metal dichalcogenide," Nat. Mater. **19**, 153–157 (2020).
[14]M. Dunz, T. Matalla-Wagner, and M. Meinert, "Spin–orbit torque induced electrical switching of antiferromagnetic MnN," Phys. Rev. Res. **2**, 013347 (2020).
[15]K. A. Omari, L. X. Barton, O. Amin, R. P. Campion, A. W. Rushforth, A. J. Kent, P. Wadley, and K. W. Edmonds, "Low-energy switching of antiferromagnetic CuMnAs/GaP using sub-10 nanosecond current pulses," J. Appl. Phys. **127**, 193906 (2020).
[16]H. Tsai, T. Higo, K. Kondou, T. Nomoto, A. Sakai, A. Kobayashi, T. Nakano, K. Yakushiji, R. Arita, S. Miwa, Y. Otani, and S. Nakatsuji, "Electrical manipulation of a topological antiferromagnetic state," Nature **580**, 608–613 (2020).
[17]T. Moriyama, K. Oda, T. Ohkochi, M. Kimata, and T. Ono, "Spin torque control of antiferromagnetic moments in NiO," Sci. Rep. **8**, 14167 (2018).
[18]X. Z. Chen, R. Zarzuela, J. Zhang, C. Song, X. F. Zhou, G. Y. Shi, F. Li, H. A. Zhou, W. J. Jiang, F. Pan, and Y. Tserkovnyak, "Antidamping-torque-induced switching in biaxial antiferromagnetic insulators," Phys. Rev. Lett. **120**, 207204 (2018).
[19]L. Baldrati, O. Gomonay, A. Ross, M. Filianina, R. Lebrun, R. Ramos, C. Leveille, F. Fuhrmann, T. R. Forrest, F. Maccherozzi, S. Valencia, F. Kronast, E. Saitoh, J. Sinova, and M. Kläui, "Mechanism of Néel order switching in antiferromagnetic thin films revealed by magnetotransport and direct imaging," Phys. Rev. Lett. **123**, 177201 (2019).

[20]I. Gray, T. Moriyama, N. Sivadas, G. M. Stiehl, J. T. Heron, R. Need, B. J. Kirby, D. H. Low, K. C. Nowack, D. G. Schlom, D. C. Ralph, T. Ono, and G. D. Fuchs, "Spin seebeck imaging of spin-torque switching in antiferromagnetic Pt/NiO heterostructures," Phys. Rev. X **9**, 041016 (2019).
[21]P. Zhang, J. Finley, T. Safi, and L. Liu, "Quantitative study on current-induced effect in an antiferromagnet insulator/Pt bilayer film," Phys. Rev. Lett. **123**, 247206 (2019).
[22]Y. Cheng, S. Yu, M. Zhu, J. Hwang, and F. Yang, "Electrical switching of tristate antiferromagnetic Néel order in alpha-Fe_2O_3 epitaxial films," Phys. Rev. Lett. **124**, 027202 (2020).
[23]A. Manchon, J. Železný, I. M. Miron, T. Jungwirth, J. Sinova, A. Thiaville, K. Garello, and P. Gambardella, "Current-induced spin–orbit torques in ferromagnetic and antiferromagnetic systems," Rev. Mod. Phys. **91**, 035004 (2019).
[24]M. S. Wörnle, P. Welter, Z. Kašpar, K. Olejník, V. Novák, R. P. Campion, P. Wadley, T. Jungwirth, C. L. Degen, and P. Gambardella, "Current-induced fragmentation of antiferromagnetic domains," arXiv:1912.05287 (2019), pp. 1–21.
[25]U. Schmid and H. Seidel, "Effect of high temperature annealing on the electrical performance of titanium/platinum thin films," Thin Solid Films **516**, 898–906 (2008).
[26]P. S. Ho and T. Kwok, "Electromigration in metals," Rep. Prog. Phys. **52**, 301–348 (1989).
[27]F. Schreiber, L. Baldrati, C. Schmitt, R. Ramos, E. Saitoh, R. Lebrun, and M. Kläui, "Concurrent magneto-optical imaging and magneto-transport readout of electrical switching of insulating antiferromagnetic thin films," Appl. Phys. Lett. **117**, 082401 (2020).
[28]C. C. Chiang, S. Y. Huang, D. Qu, P. H. Wu, and C. L. Chien, "Absence of evidence of electrical switching of the antiferromagnetic Néel vector," Phys. Rev. Lett. **123**, 227203 (2019).
[29]T. Matalla-Wagner, J.-M. Schmalhorst, G. Reiss, N. Tamura, and M. Meinert, "Resistive contribution in electrical switching experiments with antiferromagnets," arXiv:1910.08576 (2019), pp. 1–9.
[30]A. Churikova, D. Bono, B. Neltner, A. Wittmann, L. Scipioni, A. Shepard, T. Newhouse-Illige, J. Greer, and G. S. D. Beach, "Non-magnetic origin of spin Hall magnetoresistance-like signals in Pt films and epitaxial NiO/Pt bilayers," Appl. Phys. Lett. **116**, 022410 (2020).
[31]X. Zhou, X. Chen, J. Zhang, F. Li, G. Shi, Y. Sun, M. Saleem, Y. You, F. Pan, and C. Song, "From fieldlike torque to antidamping torque in antiferromagnetic Mn_2Au," Phys. Rev. Appl. **11**, 054030 (2019).
[32]J. Shi, V. Lopez-Dominguez, F. Garesci, C. Wang, H. Almasi, M. Grayson, G. Finocchio, and P. Khalili Amiri, "Electrical manipulation of the magnetic order in antiferromagnetic PtMn pillars," Nat. Electron. **3**, 92–98 (2020).
[33]T. Moriyama, W. Zhou, T. Seki, K. Takanashi, and T. Ono, "Spin–orbit-torque memory operation of synthetic antiferromagnets," Phys. Rev. Lett. **121**, 167202 (2018).
[34]J. Zelezny, H. Gao, K. Vyborny, J. Zemen, J. Masek, A. Manchon, J. Wunderlich, J. Sinova, and T. Jungwirth, "Relativistic Neel-order fields induced by electrical current in antiferromagnets," Phys. Rev. Lett. **113**, 157201 (2014).
[35]I. M. Miron, K. Garello, G. Gaudin, P.-J. Zermatten, M. V. Costache, S. Auffret, S. Bandiera, B. Rodmacq, A. Schuhl, and P. Gambardella, "Perpendicular switching of a single ferromagnetic layer induced by in-plane current injection," Nature **476**, 189–193 (2011).
[36]C. O. Avci, A. Quindeau, C.-F. Pai, M. Mann, L. Caretta, A. S. Tang, M. C. Onbasli, C. A. Ross, and G. S. D. Beach, "Current-induced switching in a magnetic insulator," Nat. Mater. **16**, 309–314 (2017).
[37]E. G. Tveten, A. Qaiumzadeh, and A. Brataas, "Antiferromagnetic domain wall motion induced by spin waves," Phys. Rev. Lett. **112**, 147204 (2014).
[38]T. Shiino, S.-H. Oh, P. M. Haney, S.-W. Lee, G. Go, B.-G. Park, and K.-J. Lee, "Antiferromagnetic domain wall motion driven by spin–orbit torques," Phys. Rev. Lett. **117**, 087203 (2016).
[39]H. Meer, F. Schreiber, C. Schmitt, R. Ramos, E. Saitoh, O. Gomonay, J. Sinova, L. Baldrati, and M. Kläui, "Direct imaging of current-induced antiferromagnetic switching revealing a pure thermomagnetoelastic switching mechanism," arXiv:2008.05219 (2020).
[40]A. S. Núñez, R. A. Duine, P. Haney, and A. H. MacDonald, "Theory of spin torques and giant magnetoresistance in antiferromagnetic metals," Phys. Rev. B **73**, 214426 (2006).
[41]Y.-T. Chen, S. Takahashi, H. Nakayama, M. Althammer, S. T. B. Goennenwein, E. Saitoh, and G. E. W. Bauer, "Theory of spin Hall magnetoresistance," Phys. Rev. B **87**, 144411 (2013).
[42]D. Hou, Z. Qiu, J. Barker, K. Sato, K. Yamamoto, S. Vélez, J. M. Gomez-Perez, L. E. Hueso, F. Casanova, and E. Saitoh, "Tunable sign change of spin Hall magnetoresistance in Pt/NiO/YIG structures," Phys. Rev. Lett. **118**, 147202 (2017).
[43]J. Fischer, O. Gomonay, R. Schlitz, K. Ganzhorn, N. Vlietstra, M. Althammer, H. Huebl, M. Opel, R. Gross, S. T. B. Goennenwein, and S. Geprägs, "Spin Hall magnetoresistance in antiferromagnet/heavy-metal heterostructures," Phys. Rev. B **97**, 014417 (2018).
[44]L. Baldrati, A. Ross, T. Niizeki, C. Schneider, R. Ramos, J. Cramer, O. Gomonay, M. Filianina, T. Savchenko, D. Heinze, A. Kleibert, E. Saitoh, J. Sinova, and M. Kläui, "Full angular dependence of the spin Hall and ordinary magnetoresistance in epitaxial antiferromagnetic NiO(001)/Pt thin films," Phys. Rev. B **98**, 024422 (2018).
[45]F. B. Hagedorn and P. M. Hall, "Right–angle bends in thin strip conductors," J. Appl. Phys. **34**, 128–133 (1963).
[46]C. Stamm, C. Murer, M. Berritta, J. Feng, M. Gabureac, P. M. Oppeneer, and P. Gambardella, "Magneto-optical detection of the spin hall effect in Pt and W thin films," Phys. Rev. Lett. **119**, 087203 (2017).
[47]J. Agustsson, U. Arnalds, A. Ingason, K. Gylfason, K. Johnsen, S. Olafsson, and J. Gudmundsson, "Growth, coalescence, and electrical resistivity of thin Pt films grown by DC magnetron sputtering on SiO_2," Appl. Surf. Sci. **254**, 7356–7360 (2008).
[48]U. Schmid, "The impact of thermal annealing and adhesion film thickness on the resistivity and the agglomeration behavior of titanium/platinum thin films," J. Appl. Phys. **103**, 054902 (2008).
[49]L. Xiao, Z. Zhao, L. Du, S. Wu, and Q. Liu, "Annealing effect on the stability of platinum thin films covered by SiO_2 or SiNx layer," in *IEEE International Conference Nano/Micro Engineered and Molecular Systems* (IEEE, 2013), Vol. 1, pp. 352–355.
[50]C.-Y. You, I. M. Sung, and B.-K. Joe, "Analytic expression for the temperature of the current-heated nanowire for the current-induced domain wall motion," Appl. Phys. Lett. **89**, 222513 (2006).
[51]A. Yamaguchi, S. Nasu, H. Tanigawa, T. Ono, K. Miyake, K. Mibu, and T. Shinjo, "Effect of Joule heating in current-driven domain wall motion," Appl. Phys. Lett. **86**, 012511 (2005).
[52]P. Luo, Z. Lu, Z. G. Zhu, Y. Z. Li, H. Y. Bai, and W. H. Wang, "Prominent β-relaxations in yttrium based metallic glasses," Appl. Phys. Lett. **106**, 031907 (2015).
[53]P. Luo, P. Wen, H. Y. Bai, B. Ruta, and W. H. Wang, "Relaxation decoupling in metallic glasses at low temperatures," Phys. Rev. Lett. **118**, 225901 (2017).
[54]S.-M. Lee and D. G. Cahill, "Heat transport in thin dielectric films," J. Appl. Phys. **81**, 2590–2595 (1997).
[55]Substrate Provided by MTI-Corporation, "Al_2O_3 single crystal sapphire boule and polished wafer" (2019), avaialbe at https://www.mtixtl.com/xtlflyers/Al2O3.pdf.
[56]N. Stojanovic, J. Yun, J. M. Berg, M. Holtz, and H. Temkin, "Model-based data analysis for thin-film thermal conductivity measurement using microelectrothermal test structures," ASME Int. Mech. Eng. Congr. Exposition Proc. **11**, 639–645 (2007).
[57]A. J. Griffin, F. R. Brotzen, and P. J. Loos, "The effective transverse thermal conductivity of amorphous Si_3N_4 thin films," J. Appl. Phys. **76**, 4007–4011 (1994).